

Squeezed Light Induced Two-photon Absorption Fluorescence of Fluorescein Biomarkers

Tian Li,^{1,2, a)} Fu Li,^{2,3} Charles Altuzarra,^{2,4} Anton Classen,^{1,2} and Girish S. Agarwal^{1,2,3}

¹⁾Department of Biological and Agricultural Engineering, Texas A&M University, College Station, TX 77843, USA

²⁾Institute for Quantum Science and Engineering, Texas A&M University, College Station, TX 77843, USA

³⁾Department of Physics and Astronomy, Texas A&M University, College Station, TX 77843, USA

⁴⁾School of Physics and Astronomy, University of Glasgow, Glasgow G12 8QQ, U.K.

(Dated: 25 June 2020)

Two-photon absorption (TPA) fluorescence of biomarkers has been decisive in advancing the fields of biosensing and deep-tissue *in vivo* imaging of live specimens. However, due to the extremely small TPA cross section and the quadratic dependence on the input photon flux, extremely high peak-intensity pulsed lasers are imperative, which can result in significant photo- and thermal damage. Previous works on entangled TPA (ETPA) with spontaneous parametric down-conversion (SPDC) light sources found a linear dependence on the input photon-pair flux, but are limited by low optical powers, along with a very broad spectrum. We report that by using a high-flux squeezed light source for TPA, a fluorescence enhancement of ~ 47 is achieved in fluorescein biomarkers as compared to classical TPA. Moreover, a polynomial behavior of the TPA rate is observed in the DCM laser dye.

Two-photon absorption (TPA) microscopy (with near-infrared illumination) is the method of choice for *in vivo* imaging of tissues down to millimeter depths¹. It bears several advantages including intrinsic high 3-D resolution due to significant TPA occurring only in close vicinity to the focal volume, reduced out-of focus bleaching, highly reduced autofluorescence, and the capability of nearly aberration-free deep-tissue focusing along with reduced absorption²⁻⁵. Unfortunately, classical TPA is an extremely inefficient process with absorption cross sections δ_r on the order of 10^{-48} cm⁴ · s/photon⁶. Therefore, TPA sensing and imaging generally requires the use of high-intensity pulsed lasers, to insure the near-simultaneous presence of two photons to induce the process^{7,8}. However, since the excitation pulse peak power is typically 10^5 times the average power, samples are prone to endure significant photo- and thermal damage^{9,10}.

In parallel, using the unique quantum energy-time entanglement characteristics of photon pairs generated by spontaneous parametric down-conversion (SPDC), the entangled TPA (ETPA) rate can be vastly enhanced^{6,11-14}, with the absorption cross section σ_e for ETPA in the range of 10^{-18} – 10^{-22} cm². Most notably, the linear dependence of ETPA on the input photon-pair flux, which was first predicted by Gea-Banacloche¹⁵ and Javanainen and Gould¹⁶, was also verified experimentally^{6,11,13,14,17,18}. It is a major advantage over the quadratic dependence of classical TPA as the need for high intensity excitation becomes obsolete. However, most current ETPA implementations with biological specimen are limited by a low flux of $\sim 10^7$ photon pairs/s^{6,11,13,14}, equivalent to only ~ 10 pW for near-infrared wavelengths. This is mostly due to loss of correlation and difficulty of tuning biphoton wavelength in the nonlinear crystals. It is also worth mentioning that a much more efficient photon pair flux generation

has been demonstrated by Jechow *et al.* using a type-0 quasi-phase-matched periodically-poled-lithium-niobate waveguide crystal¹⁹. Their photon-pair flux can be as high as $\sim 10^{11}$ photon pairs/s.

In this work, we utilize a different quantum light source that is based on the four-wave mixing (FWM) process in an atomic ⁸⁵Rb vapor cell²⁰⁻²⁶. The setup and the respective atomic level structure are shown in Fig. 1(a) and (b). The medium possesses a large third-order electric susceptibility $\chi^{(3)}$ and is pumped by a strong narrow-band continuous-wave (CW) laser at frequency ν_1 ($\lambda = 795$ nm) with a typical linewidth $\Delta\nu_1 \sim 100$ kHz. Applying an additional coherent CW seed beam at frequency $\nu_p = \nu_1 - (\nu_{HF} + \delta)$, where ν_{HF} and δ are the hyperfine splitting in the electronic ground state of ⁸⁵Rb and the two-photon detuning respectively in Fig. 1(b) (see the Supplementary Material for further experimental details), two pump photons are converted into a pair of twin photons, namely ‘probe ν_p ’ and ‘conjugate ν_c ’ photons, adhering to the energy conservation $2\nu_1 = \nu_p + \nu_c$ (see the level structure in Fig. 1(b)). The resulting ‘twin beams’ are strongly quantum-correlated and are also referred to as (seeded) two-mode squeezed light²⁷. Major advantages are narrow-band probe and conjugate beams (~ 20 MHz)^{26,28} along with a freely adjustable photon-pair flux between 10^{13} to 10^{16} photons/s^{20,21,23-26}, which is a few orders of magnitude higher than for SPDC. Also, since FWM in atomic vapors is a non-linear parametric process based on ground-state coherences²⁹, in which the main advantage arises from small two-photon detunings from real states whereas in nonlinear crystals there is no real state to which the signal or idler photon is close, the generation of quantum correlations with FWM in atomic vapors can be therefore very efficient. As can be seen from Fig. 1(c), the twin beams exhibit a intensity-difference squeezing of 6.5 dB, which is indicative of strong quantum correlations²⁷ (see the Supplementary Material for further details of the squeezing measurement).

^{a)}Electronic mail: tian.li@tamu.edu.

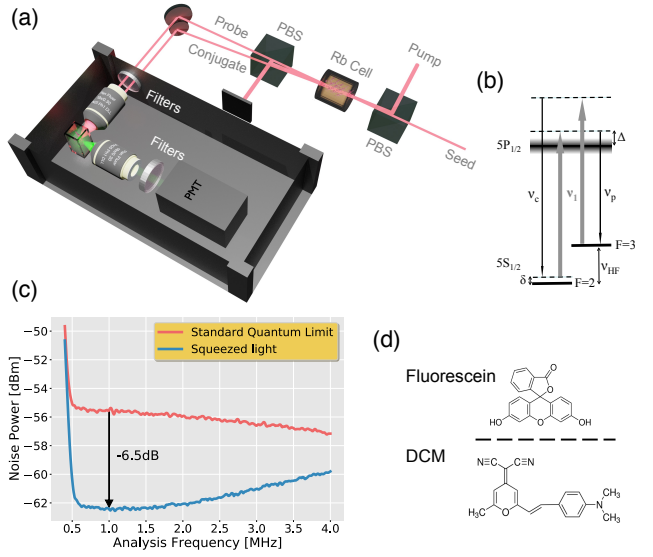


FIG. 1. (a) Squeezed-light TPA setup in which a seeded ^{85}Rb cell produces strong quantum-correlated twin beams via FWM. The twin beams are focused onto the sample with a $10\times$ objective. Fluorescence is collected at an angle of 90° with a second $10\times$ objective and fed into a photomultiplier tube (PMT). Two short-pass filters in front of the PMT exclude stray pump photons. The setup is enclosed in a light-proof box. (b) Level structure of the D1 transition of ^{85}Rb atoms. The optical transitions are arranged in a double- Λ configuration, where v_p , v_c and v_l stand for probe, conjugate and pump frequencies, respectively, fulfilling $v_p + v_c = 2v_l$. The width of the excited state in the level diagram represents the Doppler broadened line. Δ is the one-photon detuning, δ is the two-photon detuning, and v_{HF} is the hyperfine splitting in the electronic ground state of ^{85}Rb . (c) Measured intensity-difference noise power spectrum for the squeezed twin beams (blue line) and for the standard quantum limit (red line), obtained with a radio frequency spectrum analyzer (with a resolution and video bandwidth of 300 kHz and 100 Hz, respectively). A squeezing of 6.5 dB is achieved. (d) Molecular structures of fluorescein and DCM.

In this study we analyze and compare classical TPA and squeezed-light induced TPA (SL-TPA) fluorescence rates in fluorescein and DCM (see the Supplementary Material for samples preparation). Fluorescein is one of the most frequently used biomarkers for bioimaging and biosensing³⁰. Its small size is very convenient for *in vivo* imaging applications, although its relatively small classical TPA cross section generates low amounts of fluorescence^{7,8}. The SL-TPA setup is depicted in Fig. 1(a). A $10\times$ objective (Thorlabs RMS10X) focuses the near-infrared excitation light onto a solution of fluorophores. Following TPA, fluorescence is collected by a second $10\times$ objective (Thorlabs RMS10X) at an angle of 90° and guided to a photo-multiplier tube (PMT) (Thorlabs PMTSS in conjugation with a PMT transimpedance amplifier Thorlabs TIA60). Two optical low-pass filters (Thorlabs FESH0750) exclude stray pump photons. The measured PMT voltage outputs (see inset in Fig. 2) are converted into fluorescence rates of arbitrary units (since the PMT's response to an input photon is an inverse voltage pulse, adding all the inverse voltages

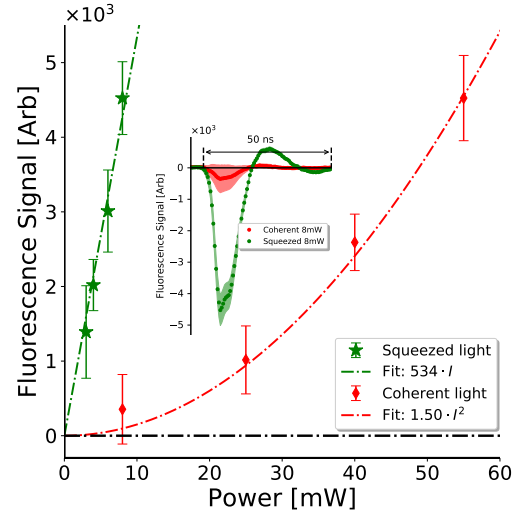


FIG. 2. Fluorescence rates versus excitation power. The red diamonds and the red (dash-dotted) line show the measured values for the coherent excitation and the respective quadratic fit. The green stars are the rates for SL-TPA induced by the twin-beam excitations, and the green (dash-dotted) line is the respective linear fit. Error bars denoting one standard deviation. Inset: raw voltage output from the PMT for coherent light (red) and squeezed light (green) excitations of 8 mW optical power. The shaded area for each curve represents one standard deviation.

in a given time window can therefore give us a quantity that is proportional to the input photon flux up to a conversion factor, see the Supplementary Material for further data acquisition details). For classical TPA measurements only the coherent pump beam is focussed into the microscope objective, with the same focus spot size at the sample. Utilized powers for the twin beams were ranging from $30 \mu\text{W}$ to the maximum of 8 mW.

Measured classical TPA fluorescence rates for fluorescein, as a function of the input power, are shown by the red diamonds in Fig. 2, with error bars denoting one standard deviation. The observed quadratic power law relationship agrees well with the established literature for classical TPA, where the fluorescence signal is proportional to the square of excitation light intensity³¹. Fluorescence rates induced by SL-TPA of 8 mW optical power (3.5 mW + 1.0 mW probe and seed; 3.5 mW conjugate) and 4 mW optical power (1.75 mW + 0.5 mW probe and seed; 1.75 mW conjugate) together with 6 mW optical power (2.6 mW + 0.8 mW probe and seed; 2.6 mW conjugate) and 3 mW optical power (1.3 mW + 0.4 mW probe and seed; 1.3 mW conjugate) are depicted by the green stars (although the 3 mW and 6 mW data points were taken on a different day, the trend is similar). Due to experimental constraints, 8 mW is the maximal power we are able to acquire for the squeezed light. The measured coherent rates are fitted by the quadratic function $R(I) = I^2 \times 1.5 \text{ mW}^{-2}$ (dash-dotted red line), which represents the benchmark of the true fluorescence rate as a function of the input power. It

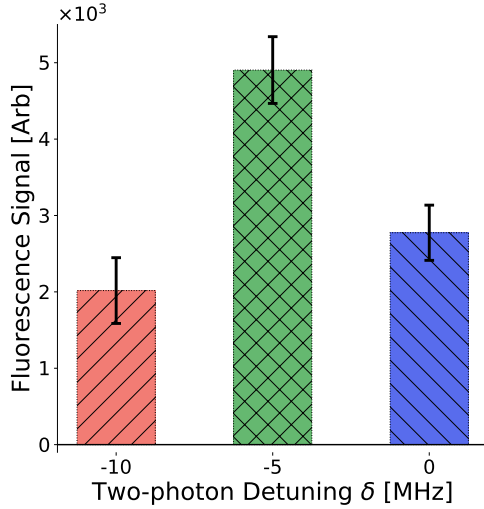


FIG. 3. Fluorescence rates for 8 mW SL-TPA with three different two-photon detunings δ , shown in the atomic level structure in Fig. 1(b) as δ . Red, green and blue bars are for $\delta = -10$ MHz, -5 MHz and 0 MHz, respectively. This figure demonstrates degraded SL-TPA enhancements as a function of the relative arrival times of the entangled photon pairs.

can be observed from the figure that the signal for 8 mW of coherent excitation deviates strongest from the fit. This fact can be attributed to background noise (e.g., electronic dark counts and spurious counts from stray ambient light) and the overall low signal to noise ratio (SNR) of the measurement (characterized by a standard deviation encompassing negative values). Following the fitted curve, the fluorescence rate for 8 mW coherent excitation is thus merely 9.6×10^1 [a.u.]. For SL-TPA of 8 mW excitation power the fluorescence rate is $\sim 4.46 \times 10^3$ [a.u.]. This value corresponds to a striking ~ 46.5 -fold enhancement over the coherent excitation. Vice versa, increasing the coherent excitation power seven-fold to ~ 55 mW, and thus the classical TPA rate by ~ 47.3 -fold, the measured rates for 8 mW SL-TPA and 55 mW classical TPA match, thus confirming the previous statement. Subtracting the contribution from the 1 mW coherent seed beam power it can be argued that the measured SL-TPA enhancement is around ~ 60 -fold over 7 mW coherent excitation. Note that the seed is uncorrelated to the quantum correlated photon pairs and that the 1 mW of coherent seed excitation itself will induce negligible classical TPA rates. More importantly, the measured fluorescence rate for 4 mW SL-TPA is $\sim 2.02 \times 10^3$ [a.u.]. Subtracting the respective optical power of the seed beam, we end up with the input flux ratio $7/3.5 = 2.00$ which matches the measured ratio $4.46/2.02 = 2.21$ well (within the calculated uncertainties). This is also true for the SL-TPA of 6 mW and 3 mW, which is indicative of the linear dependence on the input photon-pair flux that is expected for fluorescein in this regime. Quadratic terms thus do not seem to contribute here.

TPA is highly sensitive to the near-instantaneous arrival of

two photons at the sample, in particular with respect to the virtual state lifetime of the intermediate states used for the electronic transition from the ground to the final state^{13,18}. In ETPA this is quantified by the entanglement time T_e ^{6,13,32}. Adjusting T_e should change the measured SL-TPA enhancement. Hence, an investigation of the effect of relative temporal delay between the entangled photon pairs is conducted. The ETPA cross section σ_e is inversely proportional to T_e and thus the mean group velocity delay between the entangled photon pairs. In the FWM process of the atomic ^{85}Rb vapor, the group delay between the entangled pairs can be adjusted by changing the two-photon detuning δ of the double- Λ configuration in Fig. 1(b)²⁸. The red, green and blue bars in Fig. 3 show the fluorescence rates induced by 8 mW SL-TPA for the values $\delta = -10$ MHz, -5 MHz and 0 MHz, respectively. For each δ value the same relative intensity-difference squeezing of 6.5 dB (see Fig. 1(c)) is maintained, such that the results are not affected by different entanglement levels. For $\delta = -5$ MHz a relatively small delay is achieved²⁸. Degraded fluorescence rates for $\delta = -10$ MHz and $\delta = 0$ MHz confirm that the SL-TPA enhancement is degraded when the relative delay between the photon pairs is tuned away from its optimal value. Further experimental details on how to change the two-photon detuning δ can be found in the Supplementary Material.

In general, the ETPA rate R_e as a function of the input photon-pair flux density ϕ is expected to follow the functional behavior $R_e(\phi) = \sigma_e \phi + \delta_r \phi^2$, where σ_e and δ_r are the cross sections for ETPA and classical TPA respectively and are determined by the electronic level structure of the system undergoing TPA^{12,17,18,33}. Both values can be determined experimentally, or calculated theoretically via second-order perturbation theory for a sufficiently simple system¹⁸. As previously established, the coincident arrival and absorption of an entangled photon pair leads to the linear dependence $R_e(\phi) = \sigma_e \phi$ provided ϕ is sufficiently small^{6,13,14}. For sufficiently high photon-pair fluxes, TPA can be induced by uncorrelated photons from different pairs as well. The respective rate is equivalent to the classical TPA rate $\delta_r \phi^2$. Parity between both contributions is reached at the critical flux $\phi_c = \sigma_e / \delta_r$. Most previous ETPA experiments with biomarkers and low photon-pair fluxes observed only the linear dependence^{6,13,14}.

With means of investigating SL-TPA with high and freely adjustable optical powers, we investigated its functional behavior in DCM laser dye (see the Supplementary Material for its preparation). DCM dyes are known for strong TPA around 800 nm excitation wavelength, and along with a millimolar suspension, optical powers in the μW regime are sufficient to induce enough TPA fluorescence^{34,35}. The measured coherent TPA rates shown as red squares in Fig. 4, agree well with a quadratic behavior, represented by the fit function $R(I) = I^2 \times 0.304 \mu\text{W}^{-2}$. For SL-TPA in DCM, on the other hand, we observed a non-linear behavior of the functional form $R(I) = I \times 7.9 \mu\text{W}^{-1} + I^2 \times 0.59 \mu\text{W}^{-2}$. The polynomial behavior of SL-TPA in Fig. 4 implies that the photon-pair flux is already high enough to observe both linear and quadratic contributions. In fact, given the fit values, parity is already reached at $I_c = 7.9 \mu\text{W}^{-1} / 0.304 \mu\text{W}^{-2} = 26.0 \mu\text{W}$

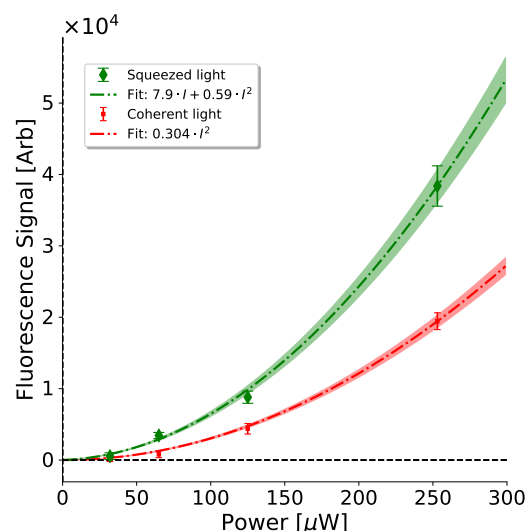


FIG. 4. Fluorescence signal of DCM versus excitation power of coherent light (red) and squeezed light (green). Coherent light fitting curve obeys a quadratic behavior, while squeezed light fitting curve shows a polynomial behavior, indicating a high input of entangled photon-pair flux.

for the DCM solution.

It is worthy to point out that the DCM laser dye solution requires much lower excitation powers than the fluorescein solution to produce appreciable TPA fluorescence rates, most probably due to a larger classical TPA cross section δ_r . In Fig. 4, the DCM signal at 130 μW coherent excitation ($\sim 0.45 \times 10^4$ a.u.) roughly equals the fluorescein signal at 55 mW coherent excitation ($\sim 4.43 \times 10^3$ a.u.). Taking into account the concentration of the two solutions (see the Supplementary Material for details of samples preparation)³⁶, we estimate the classical TPA cross section δ_r of DCM is roughly 1800 times larger than that of fluorescein. However, the ETPA cross section σ_e of DCM is actually smaller than that of fluorescein, as demonstrated by the relatively small SL-TPA enhancements. The difference can be attributed to different electronic level structures of these two organic molecules⁶.

In conclusion, this work investigates two-photon absorption fluorescence rates in fluorescein biomarkers and in DCM laser dye, induced by a coherent CW excitation light and by the bright two-mode squeezed light. For the coherent CW excitation both fluorophores show the well-expected quadratic dependence on the input photon flux. The experimental results for fluorescein with SL-TPA, however, demonstrate a linear dependence on the input optical power, along with a ~ 47 -fold TPA fluorescence enhancement for 8 mW squeezed light compared to 8 mW coherent light. This can be attributed to the predominant occurrence of entangled two-photon absorption of quantum-correlated photon pairs. In addition, and differently from previous works using quantum states of light for TPA in fluorophores, we report that SL-TPA in DCM laser dye is governed by a polynomial behavior, which can be entirely attributed to its far greater entangled photon-pair flux,

as compared to using SPDC sources. Thus, this work demonstrates that our FWM based bright two-mode squeezed light source can achieve ultra-low intensity TPA for biosensing and bioimaging, and thus bear the potential to open up unconventional avenues for *in vivo* deep tissue studies of biological specimens via TPA.

See supplementary material for complete experimental details, squeezing measurements, data acquisition and samples preparation.

The data that support the findings of this study are available from the corresponding author upon reasonable request.

This work is supported by the Air Force Office of Scientific Research (Award No. FA-9550-18-1-0141) and the Robert A. Welch Foundation (Award No. A-1943-20180324).

We thank V. Yakovlev for discussions on spectroscopy with entangled photon pairs and for the suggestion of Fluorescein biomarkers. We also thank A. Sokolov and A. Zheltikov for informative comments. A. C. acknowledges support from the Alexander von Humboldt Foundation in the framework of a Feodor Lynen Research Fellowship.

REFERENCES

- ¹F. Helmchen and W. Denk, "Deep tissue two-photon microscopy," *Nature Methods* **2**, 932 EP – (2005).
- ²J. B. Pawley, ed., *Handbook of Biological Confocal Microscopy* (Plenum, New York, 1995).
- ³C. Xu, W. Zipfel, J. B. Shear, R. M. Williams, and W. W. Webb, "Multiphoton fluorescence excitation: new spectral windows for biological nonlinear microscopy," *Proceedings of the National Academy of Sciences* **93**, 10763–10768 (1996).
- ⁴W. R. Zipfel, R. M. Williams, and W. W. Webb, "Nonlinear magic: multiphoton microscopy in the biosciences," *Nature Biotechnology* **21**, 1369–1377 (2003).
- ⁵M. Drobizhev, N. S. Makarov, S. E. Tillo, T. E. Hughes, and A. Rebane, "Two-photon absorption properties of fluorescent proteins," *Nature Methods* **8**, 393–399 (2011).
- ⁶L. Upton, M. Harpham, O. Suzer, M. Richter, S. Mukamel, and T. Goodson, "Optically excited entangled states in organic molecules illuminate the dark," *The Journal of Physical Chemistry Letters*, *The Journal of Physical Chemistry Letters* **4**, 2046–2052 (2013).
- ⁷C. Xu and W. W. Webb, "Measurement of two-photon excitation cross sections of molecular fluorophores with data from 690 to 1050 nm," *J. Opt. Soc. Am. B* **13**, 481–491 (1996).
- ⁸M. A. Albota, C. Xu, and W. W. Webb, "Two-photon fluorescence excitation cross sections of biomolecular probes from 690 to 960 nm," *Appl. Opt.* **37**, 7352–7356 (1998).
- ⁹M. A. Taylor and W. P. Bowen, "Quantum metrology and its application in biology," *Physics Reports* **615**, 1 – 59 (2016).
- ¹⁰S. N. Arkhipov, I. Saytashev, and M. Dantus, "Intravital imaging study on photodamage produced by femtosecond near-infrared laser pulses in vivo," *Photochemistry and Photobiology* **92**, 308–313 (2016).
- ¹¹J. P. Villabona-Monsalve, O. Varnavski, B. A. Palfey, and T. Goodson, "Two-photon excitation of flavins and flavoproteins with classical and quantum light," *Journal of the American Chemical Society*, *Journal of the American Chemical Society* **140**, 14562–14566 (2018).
- ¹²F. Schlawin, K. E. Dorfman, and S. Mukamel, "Entangled two-photon absorption spectroscopy," *Accounts of Chemical Research*, *Accounts of Chemical Research* **51**, 2207–2214 (2018).
- ¹³O. Varnavski, B. Pinsky, and T. Goodson, "Entangled photon excited fluorescence in organic materials: An ultrafast coincidence detector," *The Journal of Physical Chemistry Letters*, *The Journal of Physical Chemistry Letters* **8**, 388–393 (2017).

- ¹⁴J. P. Villabona-Monsalve, O. Calderón-Losada, M. Nuñez Portela, and A. Valencia, "Entangled two photon absorption cross section on the 808 nm region for the common dyes zinc tetraphenylporphyrin and rhodamine b," *The Journal of Physical Chemistry A, The Journal of Physical Chemistry A* **121**, 7869–7875 (2017).
- ¹⁵J. Gea-Banacloche, "Two-photon absorption of nonclassical light," *Phys. Rev. Lett.* **62**, 1603–1606 (1989).
- ¹⁶J. Javanainen and P. L. Gould, "Linear intensity dependence of a two-photon transition rate," *Phys. Rev. A* **41**, 5088–5091 (1990).
- ¹⁷N. P. Georgiades, E. S. Polzik, K. Edamatsu, H. J. Kimble, and A. S. Parkins, "Nonclassical excitation for atoms in a squeezed vacuum," *Phys. Rev. Lett.* **75**, 3426–3429 (1995).
- ¹⁸H.-B. Fei, B. M. Jost, S. Popescu, B. E. A. Saleh, and M. C. Teich, "Entanglement-induced two-photon transparency," *Phys. Rev. Lett.* **78**, 1679–1682 (1997).
- ¹⁹A. Jechow, A. Heuer, and R. Menzel, "High brightness, tunable biphoton source at 976 nm for quantum spectroscopy," *Opt. Express* **16**, 13439–13449 (2008).
- ²⁰M. Dowran, A. Kumar, B. J. Lawrie, R. C. Pooser, and A. M. Marino, "Quantum-enhanced plasmonic sensing," *Optica* **5**, 628–633 (2018).
- ²¹L. Cao, J. Qi, J. Du, and J. Jing, "Experimental generation of quadruple quantum-correlated beams from hot rubidium vapor by cascaded four-wave mixing using spatial multiplexing," *Phys. Rev. A* **95**, 023803 (2017).
- ²²F. Hudelist, J. Kong, C. Liu, J. Jing, Z. Y. Ou, and W. Zhang, "Quantum metrology with parametric amplifier-based photon correlation interferometers," *Nature Communications* **5**, 3049 EP – (2014).
- ²³B. E. Anderson, P. Gupta, B. L. Schmittberger, T. Horrom, C. Hermann-Avigliano, K. M. Jones, and P. D. Lett, "Phase sensing beyond the standard quantum limit with a variation on the su(1,1) interferometer," *Optica* **4**, 752–756 (2017).
- ²⁴T. Li, B. E. Anderson, T. Horrom, B. L. Schmittberger, K. M. Jones, and P. D. Lett, "Improved measurement of two-mode quantum correlations using a phase-sensitive amplifier," *Opt. Express* **25**, 21301–21311 (2017).
- ²⁵R. C. Pooser and B. Lawrie, "Ultrasensitive measurement of microcavity displacement below the shot-noise limit," *Optica* **2**, 393–399 (2015).
- ²⁶J. B. Clark, R. T. Glasser, Q. Glorieux, U. Vogl, T. Li, K. M. Jones, and P. D. Lett, "Quantum mutual information of an entangled state propagating through a fast-light medium," *Nature Photonics* **8**, 515 EP – (2014).
- ²⁷C. F. McCormick, A. M. Marino, V. Boyer, and P. D. Lett, "Strong low-frequency quantum correlations from a four-wave-mixing amplifier," *Phys. Rev. A* **78**, 043816 (2008).
- ²⁸R. T. Glasser, U. Vogl, and P. D. Lett, "Stimulated Generation of Superluminal Light Pulses via Four-Wave Mixing," *Physical Review Letters* **108**, 173902 (2012).
- ²⁹C. F. McCormick, V. Boyer, E. Arimondo, and P. D. Lett, "Strong relative intensity squeezing by four-wave mixing in rubidium vapor," *Opt. Lett.* **32**, 178–180 (2007).
- ³⁰T. Robertson, F. Bunel, and M. Roberts, "Fluorescein derivatives in intravital fluorescence imaging," *Cells* **2**, 591 (2013).
- ³¹B. R. Mollow, "Two-photon absorption and field correlation functions," *Phys. Rev.* **175**, 1555–1563 (1968).
- ³²R. d. J. León-Montiel, J. c. v. Svozilík, J. P. Torres, and A. B. U'Ren, "Temperature-controlled entangled-photon absorption spectroscopy," *Phys. Rev. Lett.* **123**, 023601 (2019).
- ³³M. R. Harpham, Ö. Süzer, C.-Q. Ma, P. Bäuerle, and T. Goodson, "Thiophene dendrimers as entangled photon sensor materials," *Journal of the American Chemical Society, Journal of the American Chemical Society* **131**, 973–979 (2009).
- ³⁴A. Jechow, M. Seefeldt, H. Kurzke, A. Heuer, and R. Menzel, "Enhanced two-photon excited fluorescence from imaging agents using true thermal light," *Nature Photonics* **7**, 973 (2013).
- ³⁵T. Scheul, C. D'Amico, I. Wang, and J.-C. Vial, "Two-photon excitation and stimulated emission depletion by a single wavelength," *Opt. Express* **19**, 18036–18048 (2011).
- ³⁶D. Tabakaev, M. Montagnese, G. Haack, L. Bonacina, J.-P. Wolf, H. Zbinden, and R. Thew, "Energy-time entangled two-photon molecular absorption," *arXiv:1910.07346* (2020).